Evaluation of SAR C-band radar vegetation indices for rice crop monitoring in Tamil Nadu, India

Haseeb Habeebulla[1], Sivasankar S[1], Arun Pratap Mishra[2,*], Sanjeevi Prasad[1], Mijing Gwra Basumatary[3], Vipin Chandra Lal[4]

[1] University of Madras, Department of Geography, India
[2] Ministry of Home Affairs, Government of India, Office of the Registrar General of India, India
[3] Gauhati University, B. Borooah College (Autonomous), Department of Geography, India
[4] University of Delhi, Dr. Bhim Rao Ambedkar College, Department of Geography, India
* Corresponding author: apmishra88.rgi@nic.in

ABSTRACT

Rice (Oryza sativa) cultivation plays a critical role in food security across Asia, where smallholder farmers depend heavily on timely information about crop development and field conditions. Monitoring these changes using optical remote sensing is constrained by persistent cloud cover during monsoon-driven growing seasons, underscoring the necessity of Synthetic Aperture Radar (SAR) for continuous observation. This study evaluates the capability of Sentinel-1 C-band SAR for tracking rice phenology in two smallholder fields in Mayiladuthurai District, Tamil Nadu, during the Late Samba season (September to January). Field-scale analysis of VV, VH, and NDVI time series for 2023–2024 captured key phenological transitions, with polarization showing a strong correlation with NDVI (Farm 1: r = 0.75; Farm 2: r = 0.73). Radar Vegetation Indices (RVI, mRVI, and RVI4S1) were computed from multi-year Sentinel-1 data (2018–2023) and compared with MODIS NDVI. Although the radar indices showed high inter-correlation (r > 0.90), their relationship with NDVI remained weak (0.15–0.30). Machine learning experiments over a 1.5 × 1.5 km region (2018–2022) demonstrated that a Linear Regression model (6.92×10^{-5}) outperformed Random Forest Regression (0.000258) in predicting RVI4S1 from VV and VH, indicating linear relationship between radar channels and the index. The study highlights the suitability of Sentinel-1 SAR-particularly VH polarization – for phenology tracking in smallholder contexts, especially where optical data are limited by cloud cover.

KEYWORDS

rice (Oryza sativa); remote sensing; Sentinel-1; radar vegetation indices; machine learning; small-scale farmers; India

Received: 30 July 2025
Accepted: 14 April 2026
Published online: 30 April 2026

Habeebulla, H., S, S., Mishra, A. P., Prasad, S., Basumatary, M. G., Lal, V. C. (2026): Evaluation of SAR C-band radar vegetation indices for rice crop monitoring in Tamil Nadu, India, e23361980.2026.6
https://doi.org/10.14712/23361980.2026.6

1. Introduction

Rice (Oryza sativa) is one of the most prominent staple foods that sustains food security around the world; it mainly grows in Asia (Muthayya et al. 2014). It is consumed by nearly half of the world's population and occupying more than 11% of cultivated land (Kumar et al. 2022). More than 90% of global rice production occurs in Asian countries, where it is primarily consumed. About 80% of the world's rice is grown by small-scale farmers with low incomes, mostly in developing countries, involving around 140 million rice-growing households (FAO 2017). Rice (Oryza sativa) is traditionally grown as an annual plant, but in tropical regions, it can survive as a perennial and produce a ratoon crop for up to 30 years. Biophysical parameters, such as biomass, yield estimation, leaf area index (LAI), and water content, are critical for farmers in rice cultivation. For instance, dry biomass can be used to estimate yield. Rice cultivation is predominantly practiced in regions with abundant rainfall and relatively low labor costs, as it is a labor-intensive crop with high water requirements. In this context, timely and accurate estimation of rice-growing areas and production in Tamil Nadu state of India is essential for effective agricultural planning, food security assessment, and environmental sustainability (Surendran et al. 2021; Udimal et al. 2017).

Traditional data on rice-growing regions, seasons, and yields are often sub-national, but current systems may not meet the data requirements for food security and policy formulation. Reliable monitoring of rice phenology and crop condition is essential (Wu et al. 2023). Rice farming is linked to various environmental aspects, from water use to climate change, due to its high methane emissions (Shen et al. 2024). Thus, long-term annual monitoring is required to study the impacts of changes in rice cultivation areas and farming practices, which are likely to evolve in the coming years to address economic and environmental challenges. The use of optical data for crop monitoring and management has been widely explored over the last two decades. Vegetation indices, such as NDVI, EVI, and LAI, from optical remote sensing observations, are majorly applied to assess crop growth stages (Omia et al. 2023). However, persistent cloud cover under monsoon-driven rice cultivation severely constrains passive optical remote sensing, leading to data gaps during critical phenological transitions. SAR is unaffected by these constraints by providing day-night, cloud-independent observations sensitive to the canopy structure, the accumulation of biomass, and conditions in field water. Moreover, the Sentinel-1 provides C-band SAR data with dual polarization (VV and VH), enabling systematic, all-weather monitoring of agricultural surfaces (ESA 2018). Various studies have proven that dual-polarimetric SAR backscatter efficiently characterizes soil and vegetation conditions over agricultural croplands (Bhogapurapu et al. 2022). These properties make Sentinel-1 especially suitable for monitoring transplanted rice systems (Atzberger 2013; Inoue et al. 2014; Wu et al. 2023).

Early studies have shown that C-band SAR backscatter is highly sensitive to rice phenological stages, especially in conditions related to flooding and canopy development (Le Toan et al. 1997). Time-series Sentinel-1 SAR data have proven effective for mapping rice extent and cropping patterns in cloud-prone deltaic environments (Nguyen et al. 2016). Temporal variation in Sentinel-1 VV and VH backscatter aligns with critical rice phenological stages, such as transplanting, vegetative growth, and maturity, supporting use of SAR for rice monitoring (Choudhury et al. 2022). Despite these advances relatively few studies have evaluated SAR performance in heterogeneous smallholder landscapes where field size, planting dates, irrigation schedules, and waterlogging vary greatly. Radar Vegetation Indices (RVIs) have been proposed to enhance crop monitoring; however, their long-term consistency and relationship to optical vegetation indices at the farm scale remain insufficiently investigated (Inoue et al. 2014; Veloso et al. 2017; Wu et al. 2023). To address these gaps, this study integrates multi-year Sentinel-1 C-band backscatter with both field-scale and multi-year NDVI time series to assess the potential of SAR for rice monitoring in two farm fields in Mayiladuthurai District, Tamil Nadu. It has been observed in previous studies that SAR times series are capable of providing complementary information to optical satellite data, such as NDVI, especially for crop structure and moisture (Blaes et al. 2005).

Random Forest regression models were employed to predict RVI4S1 using Sentinel-1 VV and VH polarization data. The effectiveness of machine learning approaches for analyzing multi-temporal Sentinel-1 SAR data in rice-growing regions has been reported in earlier studies (Onojeghuo et al. 2018). Comprehensive reviews have emphasized the importance of integrating optical and SAR data for reliable rice crop monitoring at regional and global scales (Kuenzer and Knauer 2013). A multi-year radar-optical correlations with phenological analyses at the field scale and offers an integrated evaluation of Sentinel-1 SAR data with respect to smallholder rice systems. The specific objectives of this study are to analyse field-scale phenological trajectories of rice during the 2023–2024 Late Samba season using Sentinel-1 VV and VH backscatter and Sentinel-2 NDVI, to evaluate multi-year (2018–2023) radar-optical relationships by examining correlations between MODIS NDVI and SAR-derived radar vegetation indices (RVI, mRVI, and RVI4S) and to compare machine learning models of Linear Regression and Random Forest Regression to predict RVI4S1 using VV and VH.

2. Study area

The study area is predominantly agricultural, with irrigated rice (Oryza sativa) forming the major crop and occupying most cultivated lands. The study was carried out in Arangakudi, Vadakarai village, located in Mayiladuthurai District of Tamil Nadu, India (Fig. 1). These two farmlands are cultivated with the rice (Oryza sativa) crop variety (ADT 45) on both lands. The farms have been cultivating this variety for nearly 10 years. The cultivation of rice (Oryza sativa) crops during the Late Samba period spans 135 days, from September to January. Investigation reveals that the rice (Oryza sativa) crop cultivation during the Late Samba season occurred from September 2023 to January 2024. Seedling transplantation took place on September 1, 2023, followed by transplanting on September 21, 2023. The crop matured by December 21, 2023, but harvesting was delayed until January 25, 2024, due to unexpected water logging. Originally, harvesting was planned for January 15, 2024.

3. Datasets

3.1 Google Earth Engine (GEE) datasets

3.1.1 Sentinel-2 optical data

Sentinel-2 multispectral data is accessed from European Space Agency (ESA) through GEE. The data is used for computing Normalized Difference Vegetation Index (NDVI) for vegetation monitoring during 2023–2024, 135 days cropping cycle with Band-4 (Red) and Band-8 (NIR) of 10m resolution (Drusch et al. 2012; Tucker 1979; Gorelick et al. 2017).

3.1.2 Sentinel-1 SAR C-band data

Sentinel-1 Ground Range Detected (GRD) C-band SAR data (VV and VH dual polarization) were utilized to

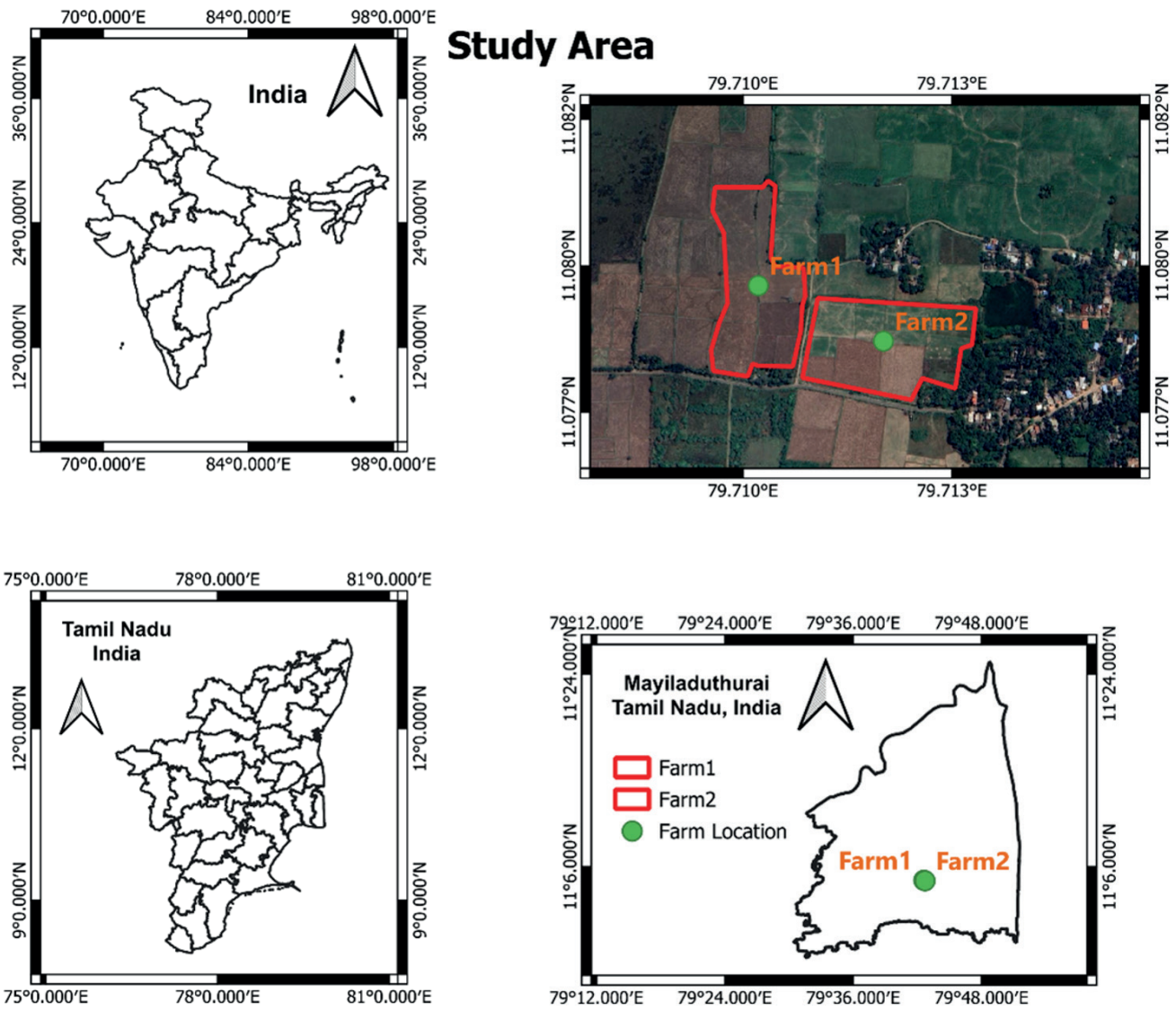

Fig. 1 Maps of locations. Farm 1: Area-Acre 7.71, Farm 2: Area-Acre 8.182.

monitor structural and moisture-related changes within irrigated rice (Oryza sativa) fields. Data were pre-processed using Sentinel-1 toolbox, thermal noise removal, radiometric calibration, terrain correction using SRTM 30 or ASTER DEM (ESA 2018; Small 2011). The terrain-corrected backscatter coefficients were converted to decibels using logarithmic scaling. VV and VH polarization channels were then extracted for further analysis. For this study, mosaic scenes corresponding to specific phenological stages of the crop 135 days growth cycle were generated, ensuring temporal alignment with optical NDVI observations. Dual-polarization of C-band SAR (VV and VH) is well suited for monitoring rice environments due to its sensitivity to surface water conditions, canopy structure, and biomass dynamics (Inoue et al. 2014; Bouvet and Le Toan 2011).

3.1.3 MODIS Terra daily NDVI

Seasonal NDVI time-series data have been widely used to map rice extent and phenological patterns in high-intensity cropping systems (Gumma et al. 2014). Multi-temporal MODIS imagery has been widely used to map paddy rice extent and seasonal dynamics across South and Southeast Asia (Xiao et al. 2006). MODIS Terra Daily NDVI product (2018–2022) was incorporated for historical vegetation trend analysis (Tab. 1). It has a coarser spatial resolution and its high temporal frequency enhances phenological assessment over multiple year (Li et al. 2024).

Tab.1 Specifications of GEE datasets.

	Dataset	Acquired
GEE	Sentinel-2A	2023–2024 (Sept, Oct, Nov, Dec, Jan)
	MODIS Terra (Daily) NDVI	2018–2023 (Sept, Oct, Nov, Dec, Jan)
	Sentinel-1 SAR GRD: C-Band	2023–2024 (Sept, Oct, Nov, Dec, Jan)

Source: ESA and NASA datasets accessed via Google Earth Engine (Gorelick et al. 2017).

4. Methodology

4.1 Phenological stages

The temporal changes in VV and VH backscatter were compared with NDVI to assess their relationship. Variations in backscatter corresponds closely changes to canopy structure and moisture content. By examining these parameters together, it is possible to identify phenological transitions, such as vegetation growth, reproductive stages, and maturity. Increases in NDVI typically align with rising VV and VH signals during biomass accumulation, while declines as the crop approaches senescence and harvest. This integrated analysis enables clearer interpretation of crop developmental stages across the 135-day growth cycle.

4.2 Correlation between different radar vegetation indices and NDVI

4.2.1 Normalized difference vegetation index (NDVI)

The NDVI used in this study was derived from the MODIS Terra Daily NDVI product (2018–2023). To enhance its suitability for Sentinel-1, the MODIS NDVI was resampled to a 10-m spatial resolution using the bilinear interpolation method. The resampled NDVI dataset was subsequently used to extract Normalized Difference Vegetation Index (NDVI) for specific dates corresponding to key stages of the 135 days crop growth cycle.

4.2.2 Radar vegetation indices

Sentinel-1 C-band VV and VH backscatter was speckle-filtered to produce Radar Vegetation Indices (RVIs). In order to ensure a physically meaningful representation of scattering intensities, the polarization values of VV and VH values were transformed from decibels (dB) to linear units using 10^ (dB/10).

- Radar Vegetation Index (RVI)
  Co- and cross-polarized backscatter intensities are used by the RVI to measure vegetation development:

$$\mathrm{RVI} = \frac{4 \cdot \mathrm{VH}}{\mathrm{VV} + \mathrm{VH}} \qquad \text{(Bhogapurapu et al.2022)}$$

  By normalizing the scattering response, this formulation produces values that ideally fall between 0 and 1. Higher values indicate more vegetation cover and larger canopy volume scattering.

- Radar vegetation index for Sentinel-1 (RVI4S1)
  The degree of polarization (DOP) is incorporated into the RVI4S1 metric to improve crop structural sensitivity:

$$q = \frac{VH}{VV}, DOP = \frac{1-q}{1+q}$$

$$\mathrm{RVI}_{4S1} = \sqrt{\mathrm{DOP}} \cdot \frac{4 \cdot \mathrm{VH}}{\mathrm{VV} + \mathrm{VH}} \quad \text{(Choudhury et al.2022)}$$

- Modified Radar Vegetation Index (mRVI)
  The mRVI is calculated as:

$$\mathrm{mRVI} = \left(\frac{\gamma^0_{\mathrm{VV}}}{\gamma^0_{\mathrm{VV}} + \gamma^0_{\mathrm{VH}}}\right)^{0.5} \left(\frac{4\,\gamma^0_{\mathrm{VH}}}{\gamma^0_{\mathrm{VV}} + \gamma^0_{\mathrm{VH}}}\right)$$

(Çolak et al. 2021)

The RVI, RVI4S1, and mRVI indices were all calculated using VV and VH. Their temporal profiles were then statistically compared with NDVI to identify which radar-based metric exhibits the strongest correspondence with vegetation crop growth dynamics.

4.3 Comparison of machine learning model of random forest Regression and linear regression

4.3.1 Random forest regression

Random Forest Regression was implemented to predict the RVI4S1 using VV and VH backscatter as input features.

$$\widehat{RVI4S1}(x) = \frac{1}{B}\sum_{b=1}^{B} \hat{y}_b\,(x)$$

This model is used for nonlinear relationships between SAR backscatter (VV, VH) and the vegetation index.

4.3.2 Linear regression

Linear Regression was used as a baseline model to quantify the linear dependency of RVI4S1 on VV and VH. A multiple linear regression model was fitted using:

$$RVI4S1 = \beta_0 + \beta_1 VV + \beta_2 VH,$$

where and represent the contribution of each polarization to the predicted vegetation index. This study-specific formulation evaluates how well simple linear combinations of VV and VH explain variability in RVI4S1, allowing direct comparison with the Random Forest model's nonlinear predictive capability.

5. Results and discussion

5.1 Phenological stages analysis

The Fig. 2 illustrates the temporal variation of VV backscatter for Farm 1 from September 2023 to January 2024. Spatial variations in backscatter intensity indicate changes in surface conditions and Oryza sativa growth stages, with marked responses at the selected field locations. The phenological graph illustrated in Fig. 3 shows seasonal variations in Oryza sativa growth for both Farm 1 and Farm 2. The decreases observed on 1 October 2023 for Farm 1 and 15 September 2023 for Farm 2 correspond to the transplanting stage, during which flooded conditions and a smooth soil-water surface reduce radar backscatter. According to farmer records, transplanting at Farm 2 occurred approximately one week later than Farm 1 due to temporary labour shortages; this temporal offset is clearly reflected in the respective backscatter profiles. Subsequent increases in signal intensity, around 30 October 2023 for Farm 1 and 15 November 2023 for Farm 2, are onset of the flowering stage, when canopy density and biomass begin to rise. For Farm 1, VV backscatter values ranging from approximately −11.147 dB to −8.788 dB between 15 November 2023 and 25 January 2024, indicating progressively stronger canopy scattering, characteristic of late reproductive to early maturity phases and approaching the harvest stage. Findings of the study align with previous research observation in the Asian context carried out by Dineshkumar and Satishkumar (2019) that demonstrated that Sentinel-1 C-band SAR data can effectively monitor rice crop growth, with volume scattering increasing and surface scattering decreasing as the crop progresses through its phenological stages. In a similar GEE-based analysis, Dineshkumar et.al (2019) showed that both scattering of VV and VH polarization were lowest during the transplanting stage and increase toward peak vegetation, demonstrating the sensitivity of SAR backscatter to rice phenological progression.

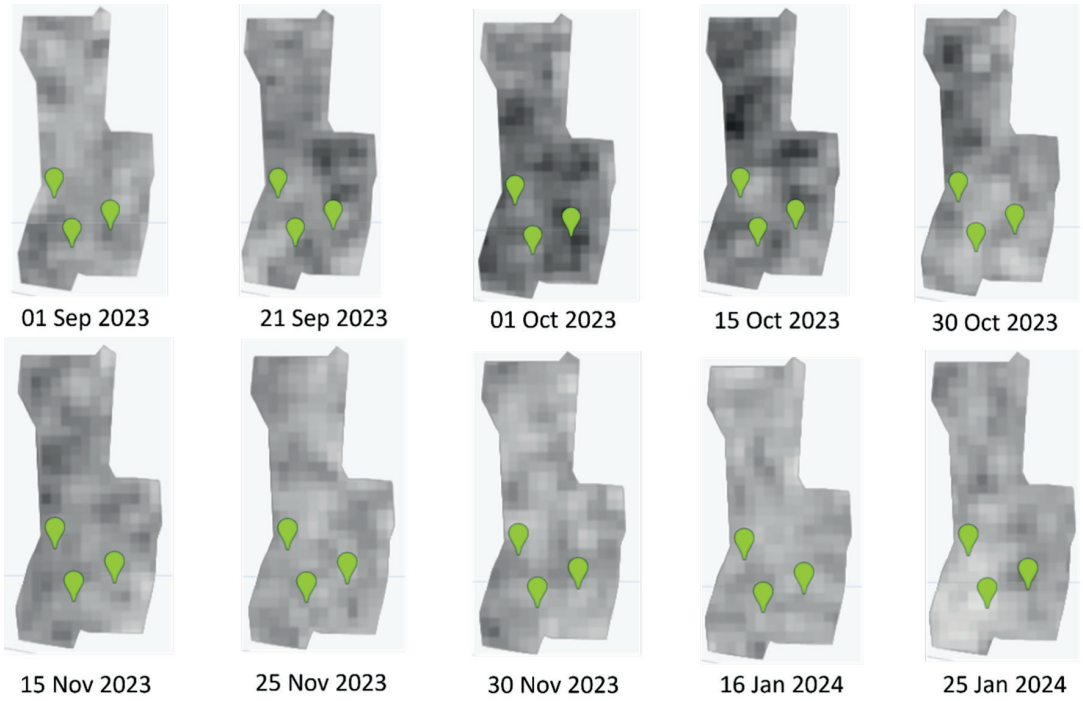

Fig. 2 VV backscatter from Farm 1 (Sep 2023–Jan 2024).

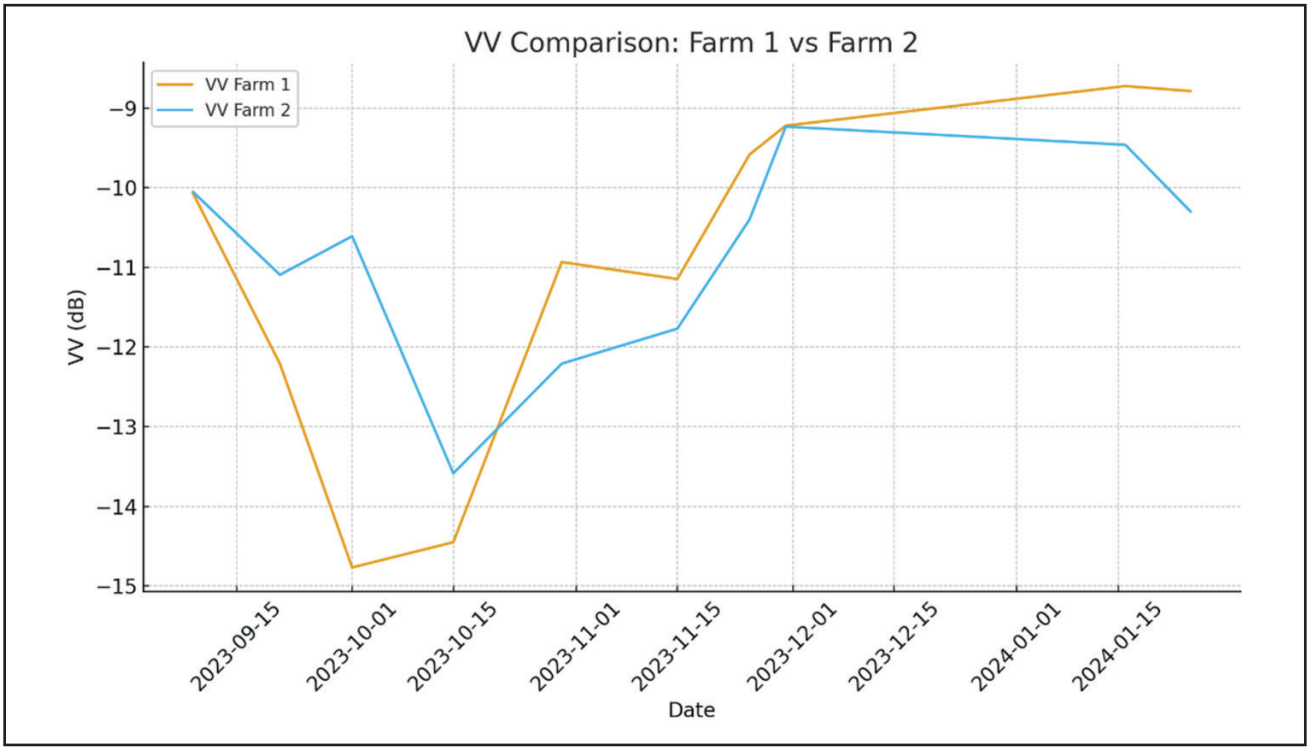

Fig. 3 VV backscatter graph from Farm 1 and Farm 2 (Sep 2023–Jan 2024).

5.2 Interpretation of VH polarization

The Fig. 4 shows multi-date VH-polarized SAR backscatter images of Farm 1 during the Oryza sativa cropping period. Variations in backscatter intensity across dates reflect changes in canopy structure and moisture conditions at the selected field locations VH backscatter for Farm 1 shows an increasing trend from −20.255 dB starting on 30 October 2023, corresponding to canopy development. The backscatter reaches a peak value of −13.51 dB on 25 January 2024, which coincides with the harvesting stage (Fig. 5). VH polarization is observed as dip associates with early growth stages characterized by low biomass and soil or surface water conditions; similarly, Mohit et al. (2022) found that VV and VH backscatter decreased during pearl millet's early growth phase and then increased as canopy development advanced. The interpretation of the observed October minimum as a transplanting and early establishment phase is supported by the increase in VH backscatter in the current study, which is consistent with increased volume scattering from the growing rice canopy.

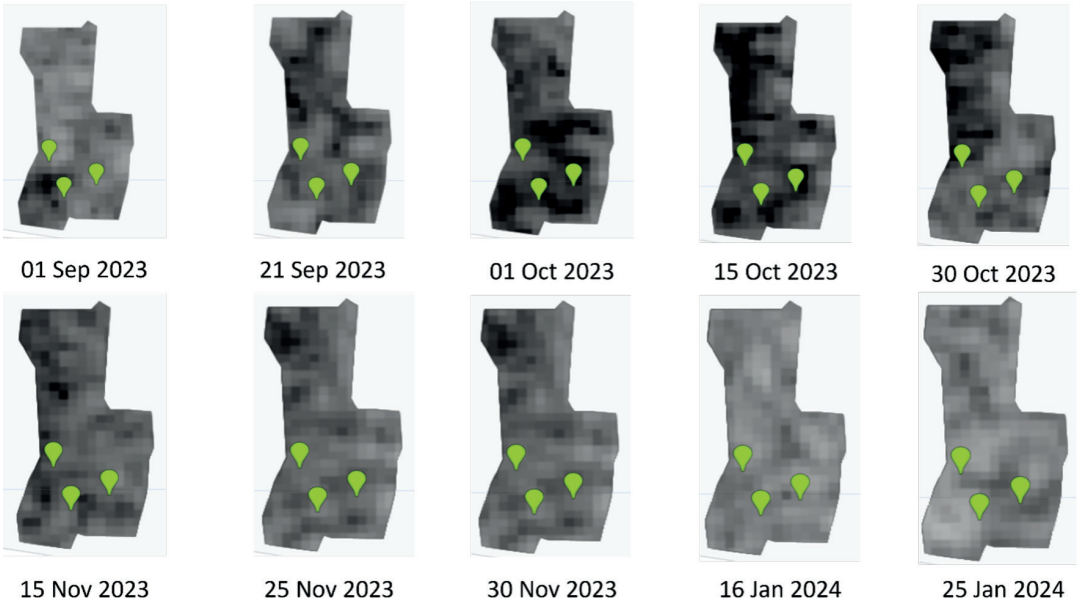

Fig. 4 VH backscatter from Farm 1 (Sep 2023–Jan 2024).

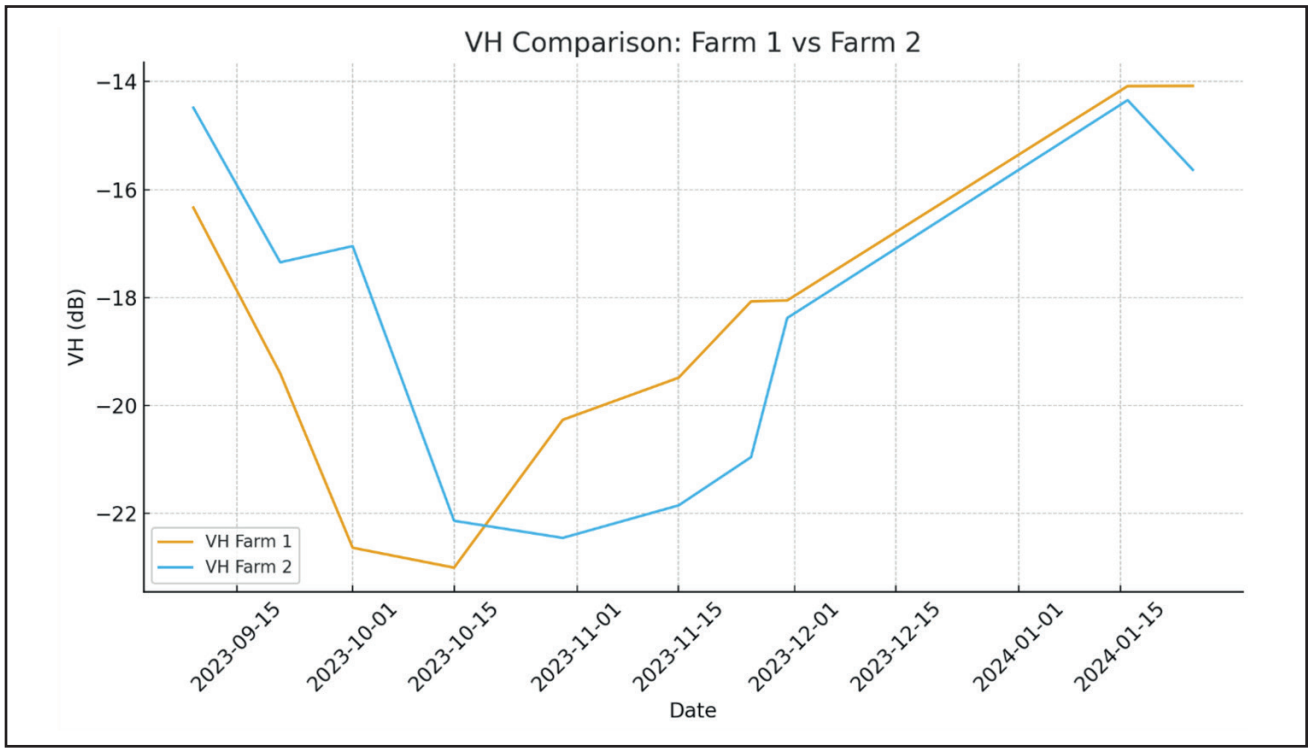

Fig. 5 VH backscatter graph from Farm 1 and Farm 2 (Sep 2023–Jan 2024).

5.3 Interpretation of NDVI

The Fig. 6 illustrates the spatial and temporal variation of SAR-based NDVI values over Farm 1 from September 2023 to January 2024. Progressive changes in NDVI intensity indicate Oryza sativa growth and canopy development at the sampled field locations. Comparing NDVI (Fig. 7) with VV (Fig. 5) and VH (Fig. 3) clearly shows the phenological transition of Farm 1 during late 2023. NDVI begins to rise after 15 November 2023 (−0.002 to 0.280 by 16 January 2024), corresponding with increasing VV backscatter (−11.147 to −8.725 dB) as canopy structure develops. In contrast, VH backscatter becomes progressively less negative (−19.487 to −14.081 dB), indicating a reduction in water-rich biomass as plants enter maturity. In correlation analysis, this shows strong associations between VH-NDVI (Pearson: 0.75; Spearman: 0.90)

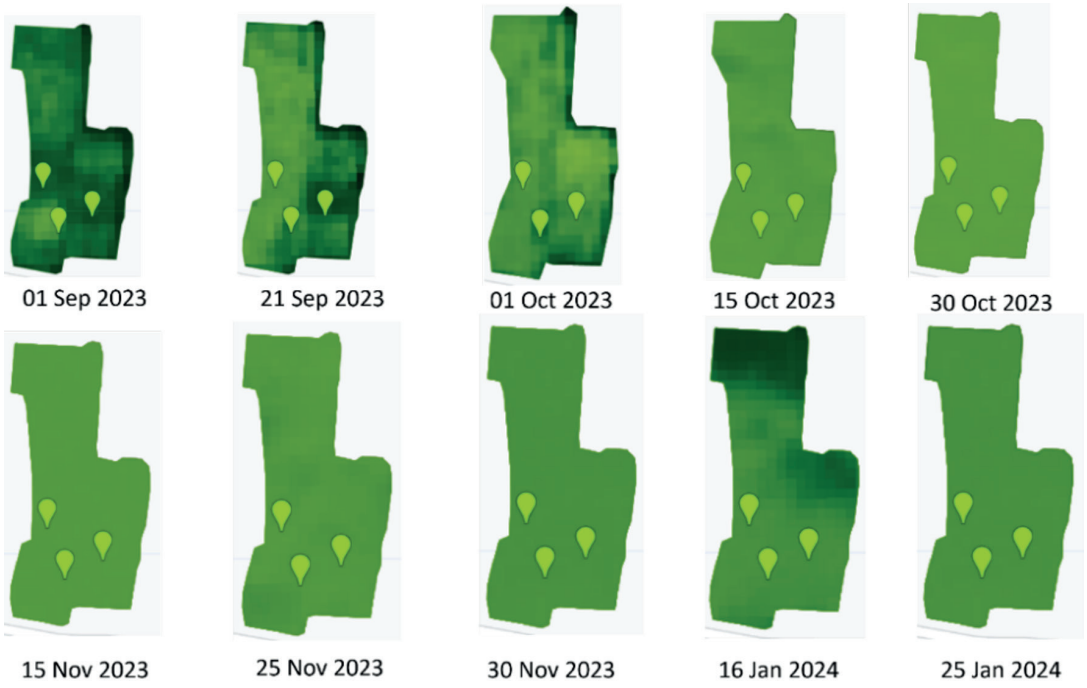

Fig. 6 NDVI from Farm 1 (Sep 2023–Jan 2024).

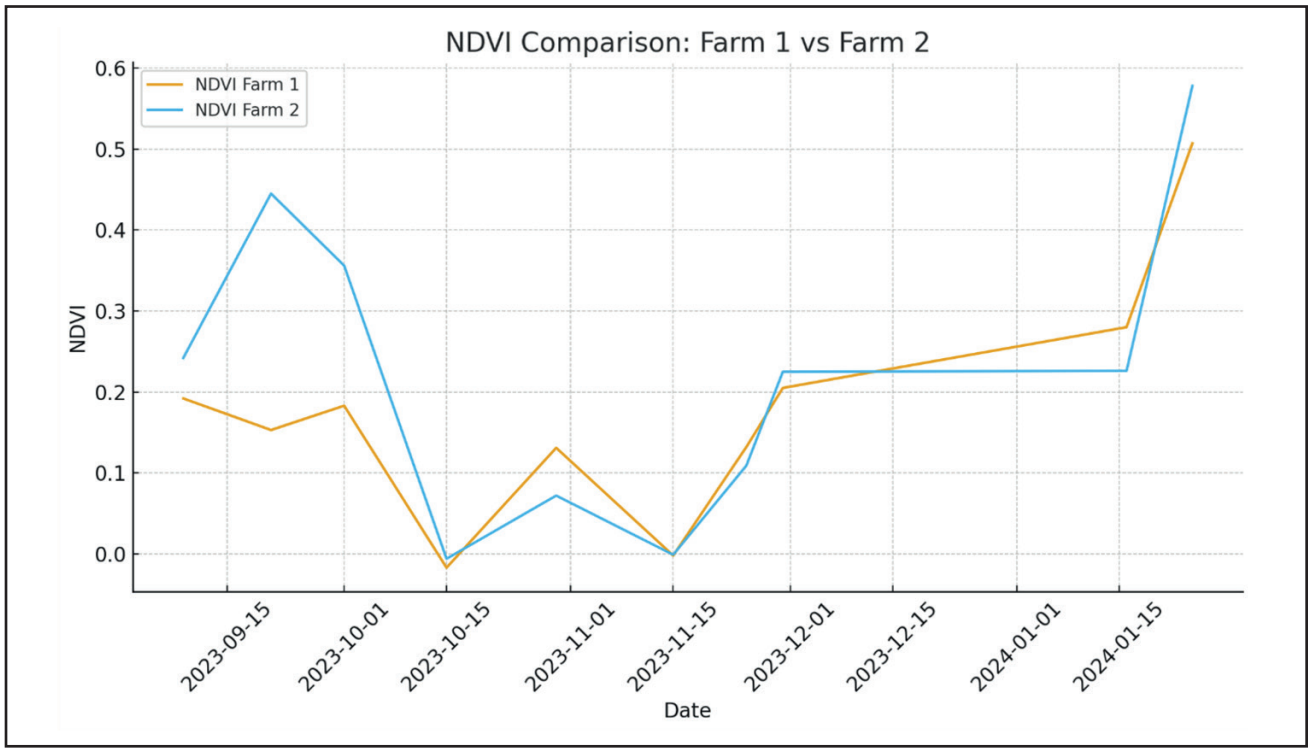

Fig. 7 NDVI graph from Farm 1 and Farm 2 (Sep 2023–Jan 2024).

Farm 1 and VH-NDVI (Pearson: 0.73; Spearman: 0.76) Farm 2, reflecting VH's sensitivity to biomass changes. The combined trends in NDVI, VV, and VH therefore confirm a decline in wet biomass after mid-November, marking the progression from reproductive growth toward harvest readiness.

5.4 Highly Correlated Radar Vegetation Index with NDVI

The Correlation Matrix data taken for the Farm 1 for the year 2018 (Sep, Oct, Nov, Dec, Jan), 2019 (Sep, Oct, Nov, Dec, Jan), 2020 (Sep, Oct, Nov, Dec, Jan), 2021 (Sep, Oct, Nov, Dec, Jan), 2022 (Sep, Oct, Nov, Dec, Jan), 2023 (Sep, Oct, Nov, Dec, Jan). The correlation matrix shows the correlation coefficients between different indices, including RVI, RVI4S1, mRVI, and NDVI (Fig. 8–10; Tab. 2). The correlation analysis reveals a strong relationship among the radar vegetation indices. RVI has a very strong positive correlation with both RVI4S1 (r = 0.95) and mRVI (r = 0.95). A slightly lower but still strong correlation exists between RVI4S1 and mRVI (r = 0.91). In contrast, the relationship between NDVI and radar-derived indices is weak. The correlation is about 0.15 for both RVI and mRVI, and 0.21 for RVI4S1. Of all the radar indices, RVI4S1 exhibits the strongest correlation with NDVI. This indicates that RVI4S1 is the most sensitive SAR-based index to vegetation variations recorded by optical NDVI.

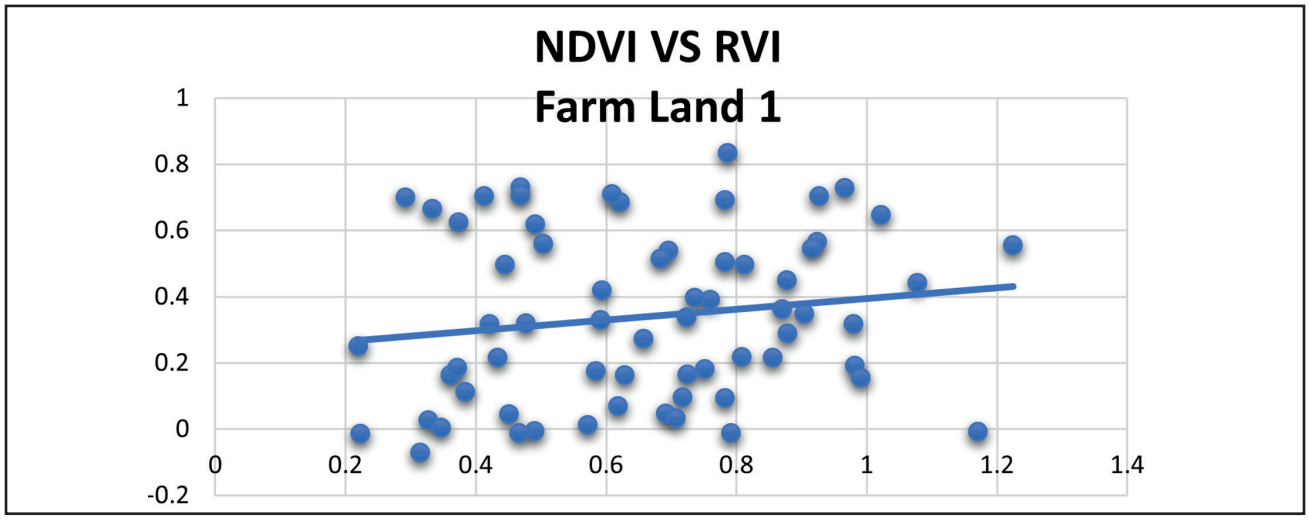

Fig. 8 Correlation between NDVI and RVI for Farm 1 (Sep 2018–Jan 2024).

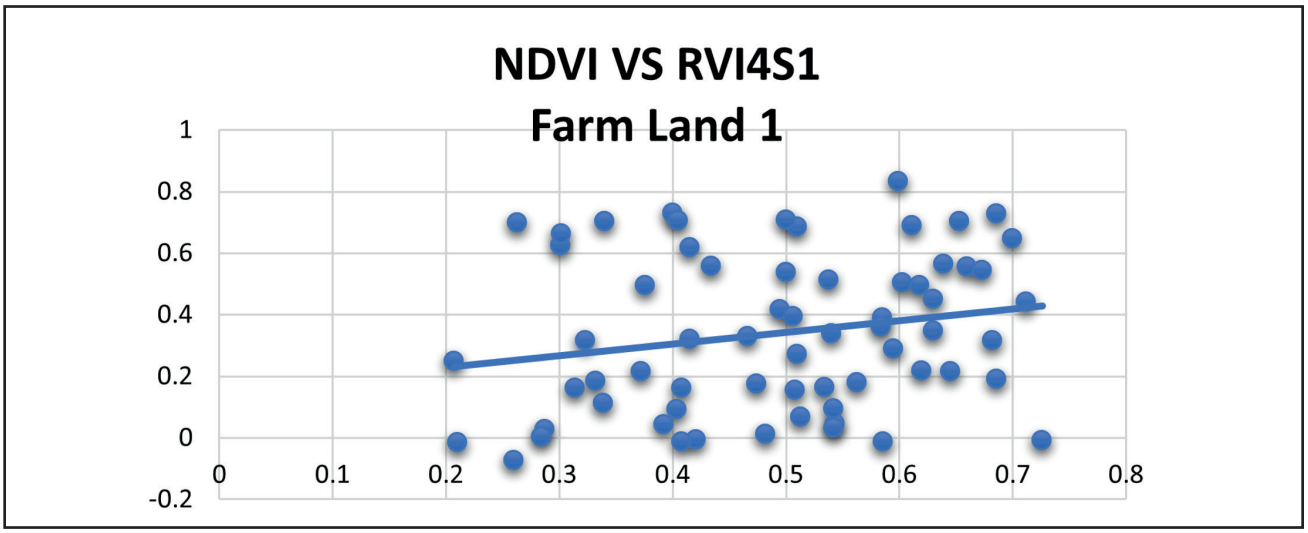

Fig. 9 Correlation between NDVI and RVI4S1 for Farm 1 (Sep 2018–Jan 2024).

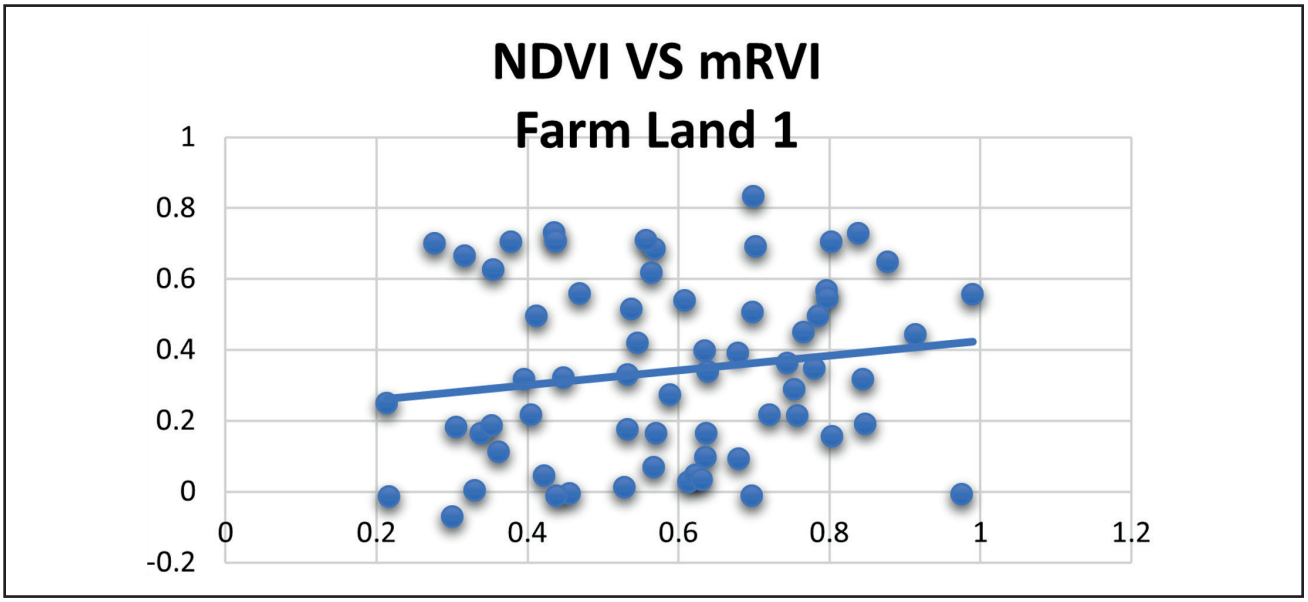

Fig. 10 Correlation between NDVI and mRVI for Farm 1 (Sep 2018–Jan 2024).

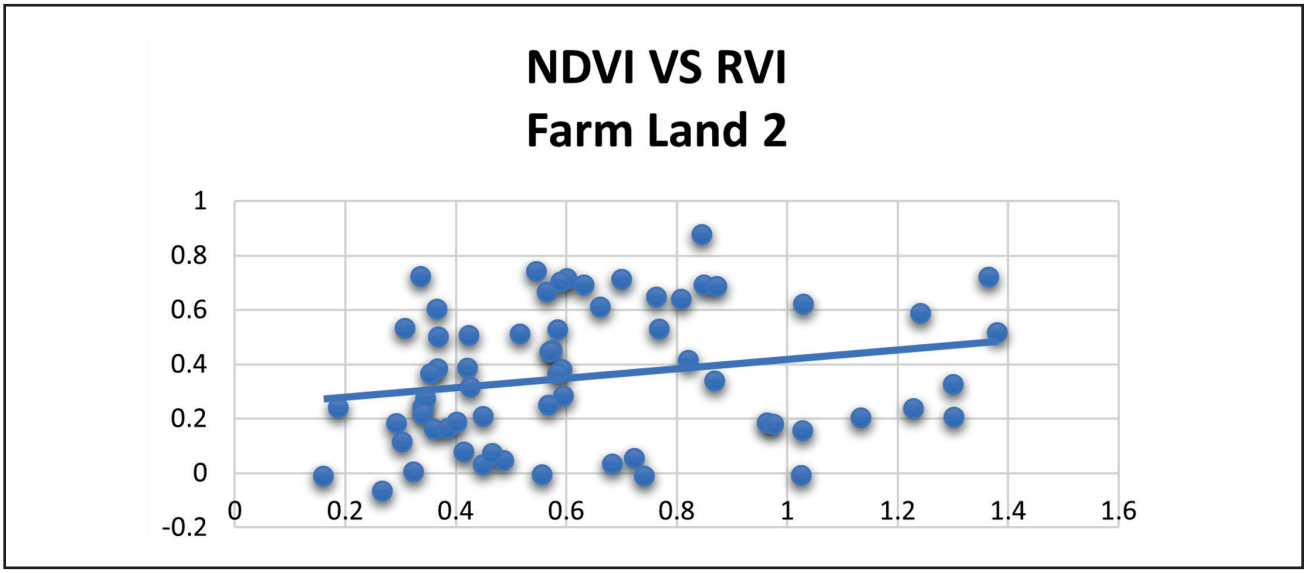

Fig. 11 Correlation between NDVI and RVI for Farm 2 (Sep 2018–Jan 2024).

Tab. 2 Farm 1 correlation matrix for year (2018–2024).

	RVI	RVI4S1	mRVI	NDVI
RVI	1			
RVI4S1	0.947171	1		
mRVI	0.948482	0.908005	1	
NDVI	0.145436	0.211982	0.149054	1

In this study, the correlation analysis in Farm 2 shows a high degree of relationship among the radar vegetation indices (Fig. 11–13; Tab. 3). There is a very high positive relationship between RVI and both RVI4S1 (r = 0.96) and mRVI (r = 0.97). This establishes a high degree of similarity among the above three SAR vegetation indices. There is also a high level of similarity between RVI4S1 and mRVI (r = 0.94). Conversely, the other three vegetation indices (RVI, mRVI, and RVI4S1) show a low degree of similarity with the optical vegetation index of NDVI. The correlation coefficient values are estimated to be about 0.22 in the case of RVI, 0.19 in the case of mRVI, and 0.31 in the case of RVI4S1. Out of the three radar vegetation indices, RVI4S1 shows the highest similarity with the vegetation index of NDVI. This explains that the above index has the highest similarity with vegetation activities.

Tab. 3 Farm 2 correlation matrix for year (2018–2024).

	RVI	RVI4S1	mRVI	NDVI
RVI	1			
RVI4S1	0.962686	1		
mRVI	0.969511	0.936074	1	
NDVI	0.216434	0.305704	0.193061	1

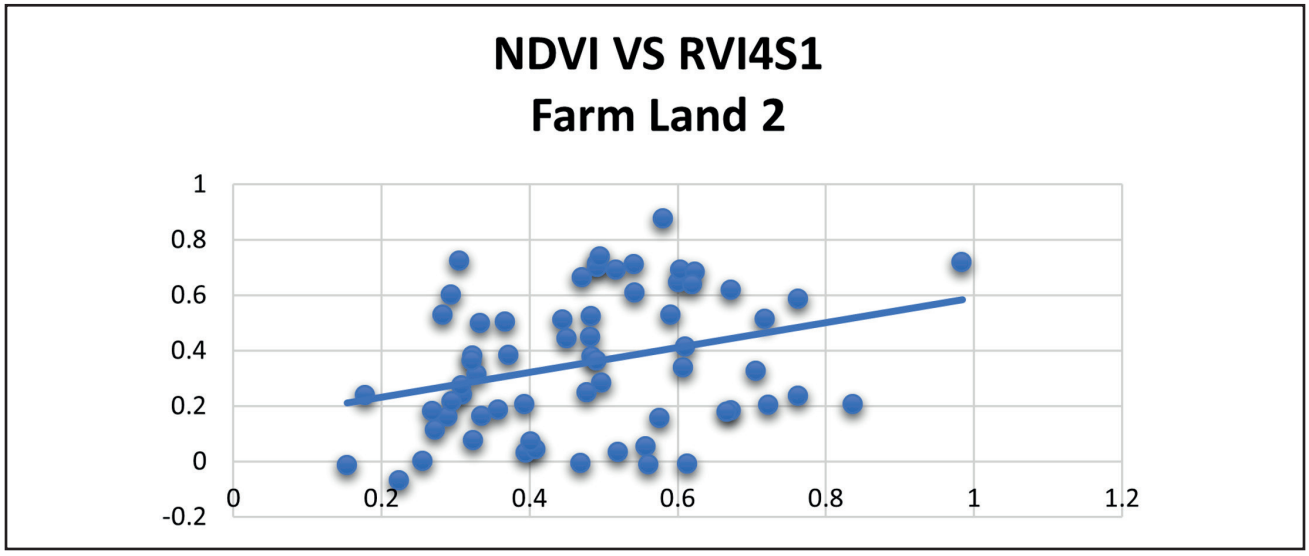

Fig. 12 Correlation between NDVI and RVI4S1 for Farm 2 (Sep 2018–Jan 2024).

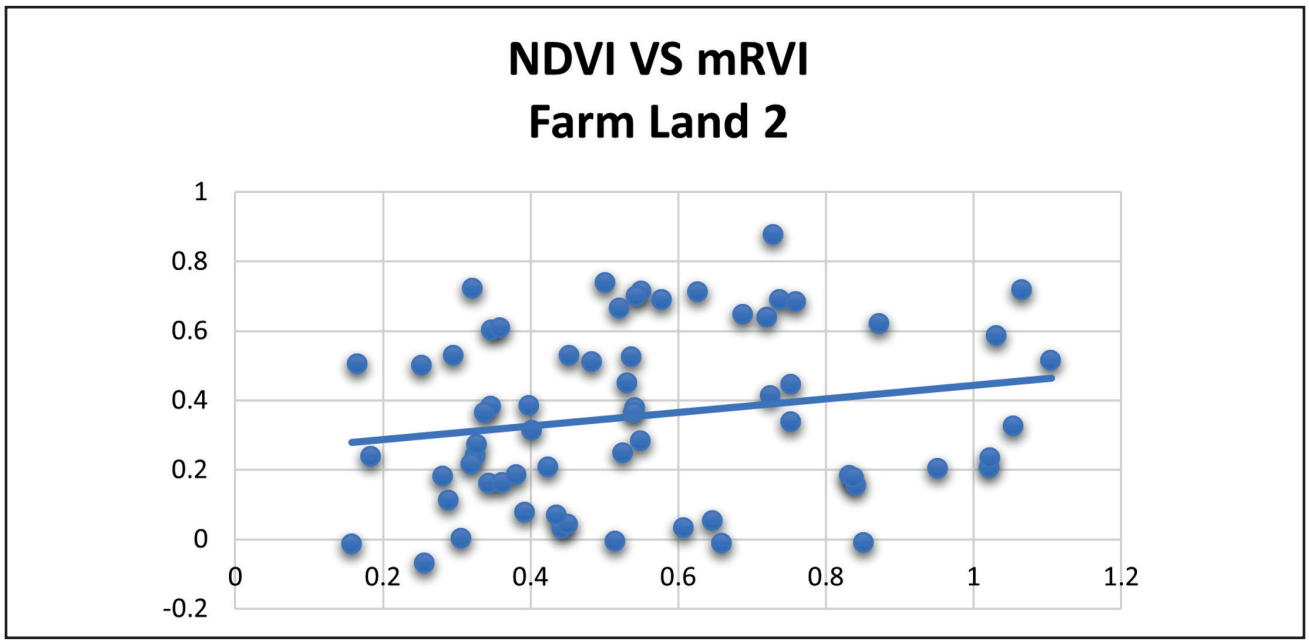

Fig. 13 Correlation between NDVI and mRVI for Farm 2 (Sep 2018–Jan 2024).

5.5 Machine learning-based analysis using random forest and linear regression on ROI mean VV, VH, and RVI4S1 data

The analysis has been performed using machine learning based on the mean backscatter values derived from a 1.5 × 1.5 km region of interest (ROI) (Fig. 14). The data involves average values of Sentinel 1, in VV, VH, as well as RV4S1, for the area of study, during 2018–2022, as illustrated in Tab. 4. Average values for every ROI, as well as every acquisition date, are one thing that is observable in the data. The latitude and longitude are retained since it is an important location parameter. The objective for the machine learning task entailed making predictions for RVI4S1, which would depend on the VV and VH values of backscatter using the Random Forest Regression (RFR) model, in addition to the Linear Regression model. The two models would operate on the same set of data. Fig. 15 shows the Plot of observed and predicted RVI4S1 values of RFR model. The mean squared error (MSE) obtained by the RFR model is 0.000258, which indicates that it works well, but it sometimes performs irregularly. The Linear Regression model outcome is represented by Fig. 16, which shows that there is good correlation between the actual and predicted values of RVI4S1. The mean squared error, 6.92×10^{-5}, is greatly reduced by the Linear Regression model, thereby proving that it is more accurate compared to the Random Forest model. The fact that the mean squared error is smaller in the Linear Regression model suggests that the linear correlation of RVI4S1 is mainly linear to VV and VH backscattering. Hence, it can be inferred that Linear Regression works better than Random Forest Regression in predicting RVI4S1.

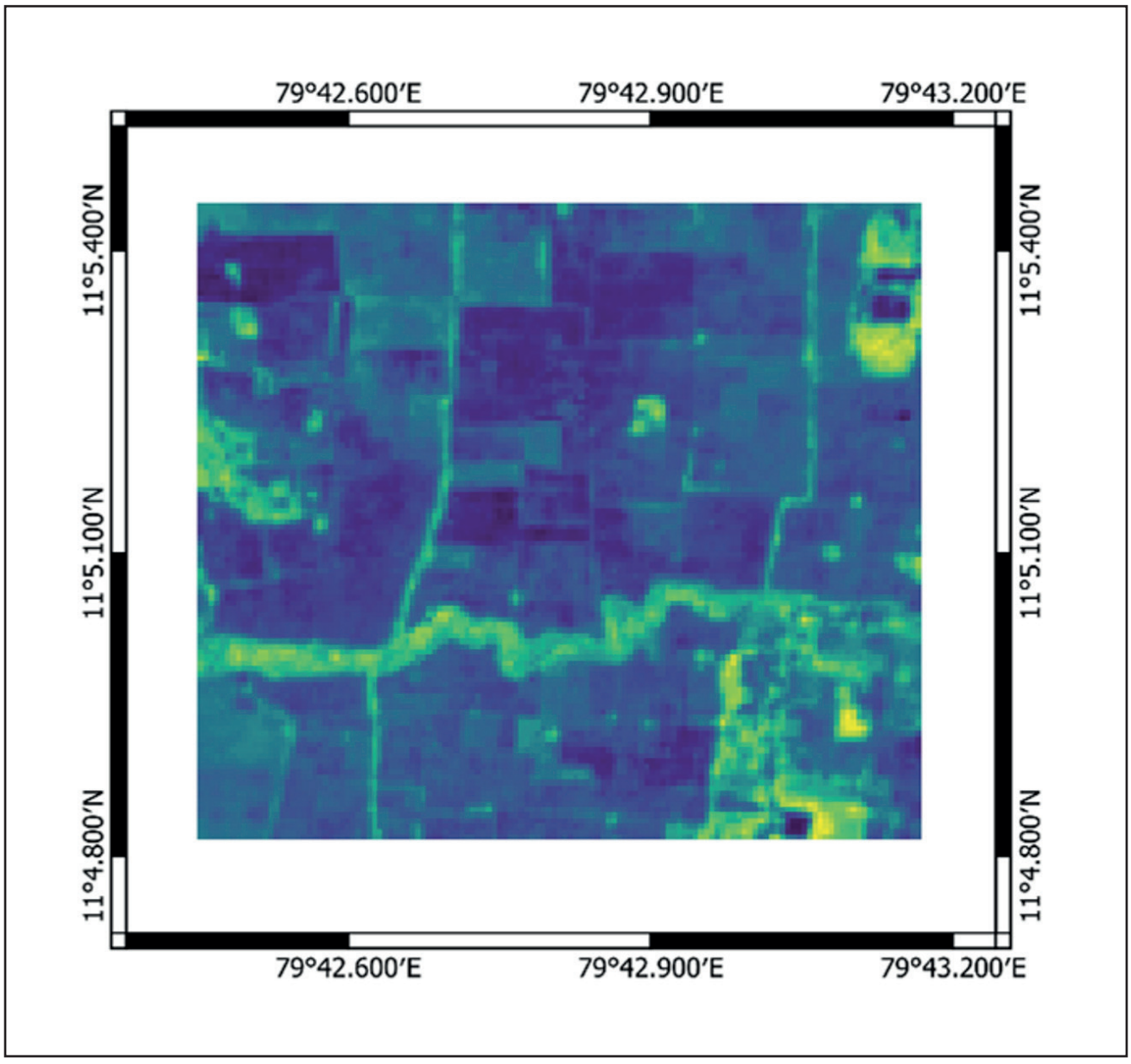

Fig. 14 Study area for ML 1.5 × 1.5 sq.km.

Tab. 4 Dataset of VV, VH, RVI4S1 (mean value study area).

Date	VH	VV	RVI4S1	Latitude	Longitude
09-09-2018	−17.3979	−9.37856	0.467578	11.0793	79.71018
21-09-2018	−23.3393	−15.0424	0.469467	11.0793	79.71018
03-10-2018	−22.937	−12.8425	0.360679	11.0793	79.71018
27-10-2018	−18.6237	−10.0553	0.447358	11.0793	79.71018
08-11-2018	−16.092	−9.59329	0.573938	11.0793	79.71018
20-11-2018	−15.555	−9.07016	0.578037	11.0793	79.71018
02-12-2018	−14.5366	−9.81567	0.661762	11.0793	79.71018
14-12-2018	−15.4968	−9.92271	0.617427	11.0793	79.71018
26-12-2018	−15.0288	−9.72776	0.650841	11.0793	79.71018
07-01-2019	−15.2461	−10.7951	0.676116	11.0793	79.71018
19-01-2019	−15.42	−9.66462	0.625057	11.0793	79.71018
31-01-2019	−14.6419	−9.51988	0.649853	11.0793	79.71018
12-02-2019	−16.4884	−10.2188	0.57928	11.0793	79.71018
24-02-2019	−16.3255	−11.302	0.659398	11.0793	79.71018

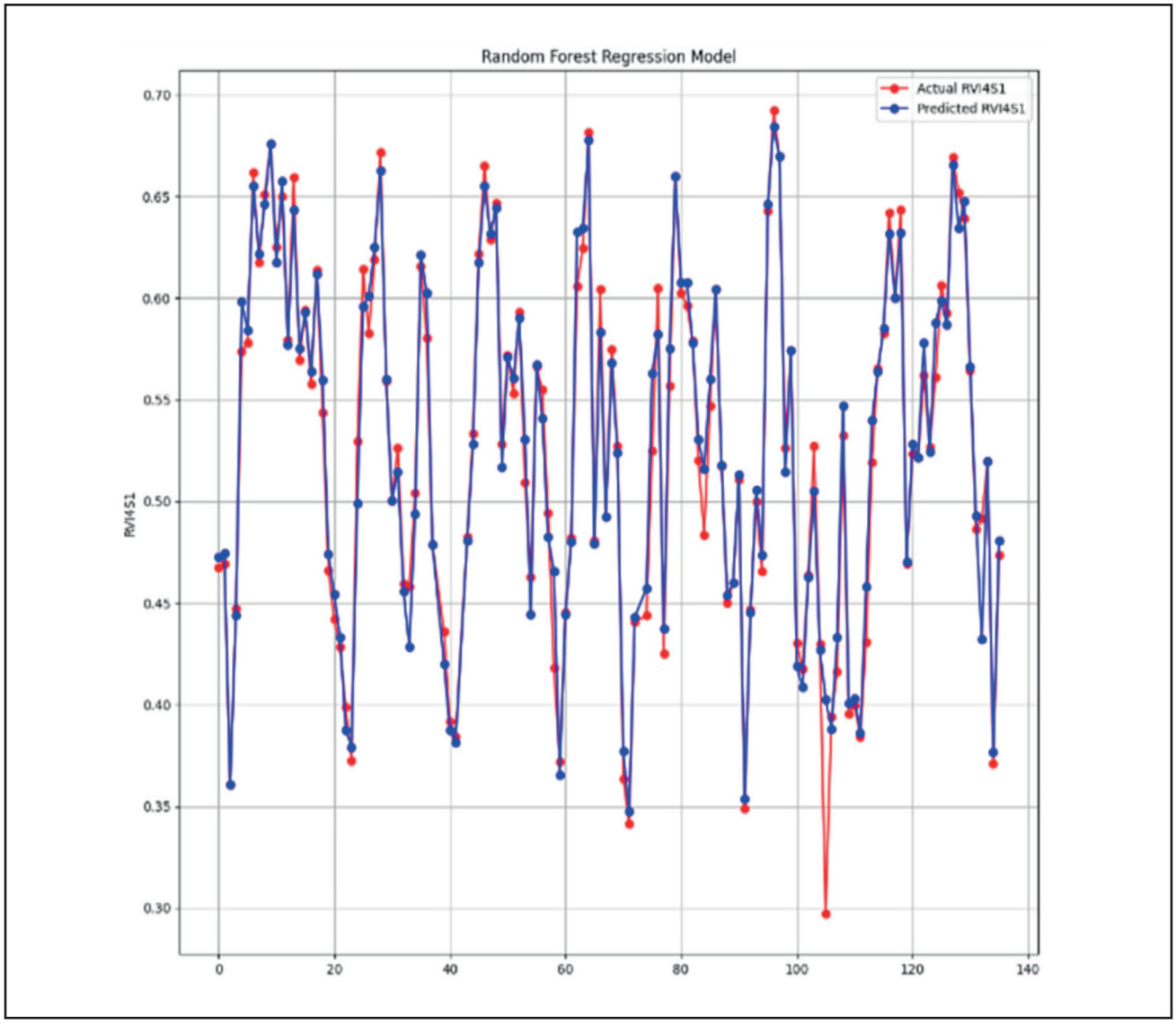

Fig. 15 Actual RVI4S1 and predicted RVI4S1 using random forest regression (Mean ROI).

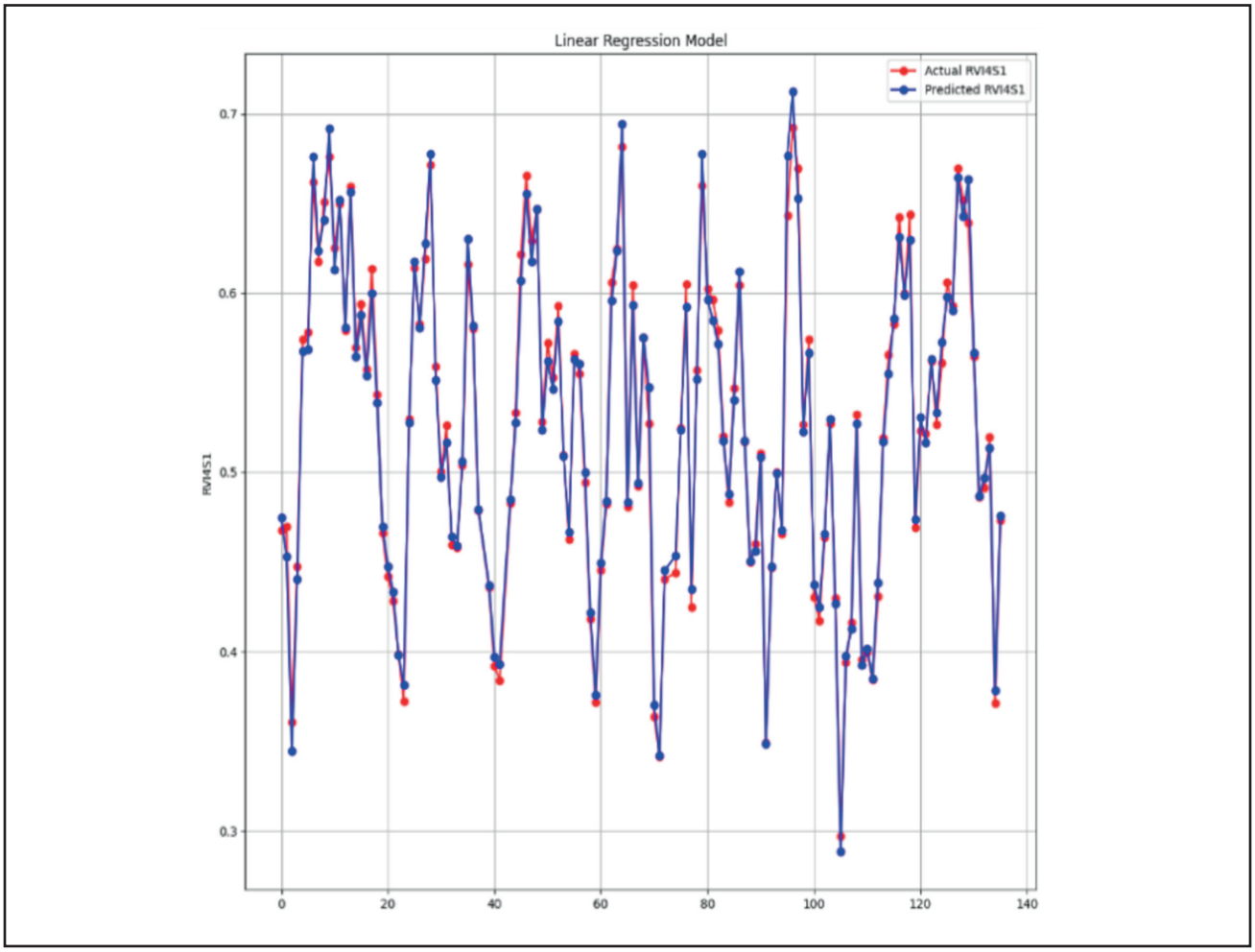

Fig. 16 Actual RVI4S1 and predicted RVI4S1 using linear regression (Mean ROI).

6. Conclusion

By combining multi-year radar backscatter, multi-year MODIS NDVI, optical and SAR measurements, this study assessed the feasibility of Sentinel-1 C-band SAR for tracking rice phenology and vegetation dynamics in two smallholder fields. VV and VH backscatter successfully capture important developmental stages, including transplanting, vegetative growth, flowering, and maturity, according to the phenological analysis for the 2023–2024 Late Samba season. VH showed especially great sensitivity to biomass and canopy moisture. Its dependability for identifying phenological transitions based on Pearson and Spearman correlations between VH and NDVI (up to 0.75 and 0.90 in Farm 1, 0.73 and 0.76 in Farm 2). Among the three Radar Vegetative Indices (RVI, mRVI, RVI4S1) exhibited strong internal correlation ($r > 0.90$) but only weak correlation with MODIS NDVI among three RVI4S1 has weak positive correlation (0.20–0.30). This indicates that radar indices primarily capture structural and moisture-related scattering, whereas NDVI represent optical greenness. The Machine Learning comparison showed that Linear Regression predicted with lower MSE than Random Forest Regression which indicates that VV, VH has Linear Relationship with RVI4S1. The result support the integration of SAR-based phenology tracking and simple linear modelling as effective, scalable tools for smallholder rice monitoring in monsoon-prone region.

Acknowledgment

This research was conducted with minimal external assistance. The authors are thankful to the editor and the anonymous learned reviewers for the insightful comments that were helpful in significantly improving the scientific quality of this research paper. The authors also acknowledge ESA and NASA for providing open-source data. We acknowledge the academic and professional resources that have contributed to shaping the understanding of the topic.

References

Atzberger, C. (2013): Advances in remote sensing of agriculture. Remote Sensing 5(2), 949–981, https://doi.org/10.3390/rs5020949.

Bhogapurapu, N., Dey, S., Mandal, D., Bhattacharya, A., Karthikeyan, L., McNairn, H., Rao, Y. S. (2022): Soil moisture retrieval over croplands using dual-pol L-band GRD SAR data. Remote Sensing of Environment 271: 112900, https://doi.org/10.1016/j.rse.2022.112900.

Blaes, X., Vanhalle, L., Defourny, P. (2005): Efficiency of Crop identification based on optical and SAR image time series. Remote Sensing of Environment 96 (3–4), 352–365, https://doi.org/10.1016/j.rse.2005.03.010.

Bouvet, A., Le Toan, T. (2011): Use of ENVISAT/ASAR wide-swath data for timely rice fields mapping in the Mekong River Delta. Remote Sensing of Environment 115(4), 1090–1101, https://doi.org/10.1016/j.rse.2010.12.014.

Choudhury, A., Mahammood, V., Rao, K. H. V. D. (2022): Rice mapping and various stages of rice growth using Sentinel-1 SAR Data-A case study of Mahabubnagar District, Telangana. International Journal of Recent Technology and Engineering 11(3), 97–100, https://doi.org/10.35940/ijrte.c7259.0911322.

Çolak, E., Chandra, M., Sunar, F. (2021): The Use of Sentinel 1/2 Vegetation Indexes with Gee Time Series Data in Detecting Land Cover Changes in the Sinop Nuclear Power Plant Construction Site. The International Archives of the Photogrammetry, Remote Sensing and Spatial Information Sciences, XLIII-B3-2021, 701–706, https://doi.org/10.5194/isprs-archives-XLIII-B3-2021-701-2021.

Dineshkumar, C., Satishkumar, J. (2019): Rice Crop Monitoring Using Sentinel-1 C-Band Data. The International Archives of the Photogrammetry, Remote Sensing and Spatial Information Sciences XLII-3/W6, 73–77, https://doi.org/10.5194/isprs-archives-XLII-3-W6-73-2019.

Dineshkumar, C., Kumar, J. S., Nitheshnirmal, S. (2019): Rice Monitoring Using Sentinel-1 Data in the Google Earth Engine Platform. Proceedings 24(1): 4, https://doi.org/10.3390/IECG2019-06206.

Drusch, M., Del Bello, U., Carlier, S., Colin, O., Fernandez, V., Gascon, F., Hoersch, B., Isola, C., Laberinti, P., Martimort, P., Meygret, A., Spoto, F., Sy, O., Marchese, F., Bargellini, P. (2012): Sentinel-2: ESA's Optical High-Resolution Mission for GMES Operational Services. Remote Sensing of Environment 120, 25–36, https://doi.org/10.1016/j.rse.2011.11.026.

European Space Agency (ESA) (2024): Sentinel-1: Radar vision for Copernicus. Available online: https://www.esa.int/Applications/Observing_the_Earth/Copernicus/Sentinel-1 (accessed on 15 December 2024).

Food and Agriculture Organization of the United Nations (FAO) (2017): Rice Market Monitor. Food and Agriculture Organization of the United Nations XX (4). Available online: https://reliefweb.int/report/world/fao-rice-market-monitor-december-2017-volume-xx-issue-no-4 (accessed on 20 March 2025).

Gorelick, N., Hancher, M., Dixon, M., Ilyushchenko, S., Thau, D., Moore, R. (2017): Google Earth Engine: Planetary-scale geospatial analysis for everyone. Remote Sensing of Environment 202, 18–27, https://doi.org/10.1016/j.rse.2017.06.03.

Gumma, M. K., Thenkabail, P. S., Maunahan, A., Islam, S., Nelson, A. (2014): Mapping seasonal rice cropland extent and area in the high cropping intensity environment of Bangladesh using MODIS 500m data for the year 2010. ISPRS Journal of Photogrammetry and Remote Sensing 91, 98–113, https://doi.org/10.1016/j.isprsjprs.2014.02.007.

Inoue, Y., Sakaiya, E., Wang, C. (2014): Capability of C band backscattering coefficients from high-resolution satellite SAR sensors to assess biophysical variables in paddy rice. Remote Sensing of Environment 140, 257–266, https://doi.org/10.1016/j.rse.2013.09.001.

Kuenzer, C., Knauer, K. (2013): Remote Sensing of Rice Crop Areas. International Journal of Remote Sensing 34(6), 2101–2139, https://doi.org/10.1080/01431161.2012.738946.

Kumar, D., Ramesh, K., Jinger, D., Rajpoot, S. K. (2022): Effect of potassium fertilization on water productivity, irrigation water use efficiency, and grain quality under direct seeded rice-wheat cropping system. Journal of Plant Nutrition 45(13), 2023–2038, https://doi.org/10.1080/01904167.2022.2046071.

Le Toan, T., Ribbes, F., Wang, L. F., Floury, N., Ding, K. H., Kong, J. A., Fujita, M., Kurosu, T. (1997): Rice crop mapping and monitoring using ERS-1 data based on experiment and modeling results. IEEE Transactions on Geoscience and Remote Sensing 35(1), 41–56, https://doi.org/10.1109/36.551933.

Li, H., Cao, Y., Xiao, J., Yuan, Z., Hao, Z., Bai, X., Wu, Y., Liu, Y. (2024): A daily gap-free normalized difference vegetation index dataset from 1981 to 2023 in China. Scientific Data 11: 527, https://doi.org/10.1038/s41597-024-03364-3.

Mohit, K., Akash, G., Neeti, N., Maity, S., Mukesh, K., Chowdary, V. M., Bimal, B., Jha, C. S., Kumar, R. (2022): Machine learning-based meta-classifier for Kharif Bajra (pearl millet) discrimination in mixed cropping environments using multi-temporal SAR data. Geocarto International 37(27), 16671–16686, https://doi.org/10.1080/10106049.2022.2113452.

Muthayya, S., Sugimoto, J. D., Montgomery, S., Maberly, G. F. (2014): An overview of global rice production, supply, trade, and consumption. Annals of the New York Academy of Sciences 1324 (1), 7–14, https://doi.org/10.1111/nyas.12540.

Nguyen, D. B., Gruber, A., Wagner, W. (2016): Mapping rice extent and cropping scheme in the Mekong Delta using Sentinel-1A data. Remote Sensing Letters 7(12), 1209–1218, https://doi.org/10.1080/2150704X.2016.1225172.

Omia, E., Bae, H., Park, E., Kim, M. S., Baek, I., Kabenge, I., Cho, B. K. (2023): Remote Sensing in Field Crop Monitoring: A Comprehensive Review of Sensor Systems, Data Analyses and Recent Advances. Remote Sensing 15(2): 354, https://doi.org/10.3390/rs15020354.

Onojeghuo, A. O., Blackburn, G. A., Wang, Q., Atkinson, P. M., Kindred, D., Miao, Y. (2018): Mapping paddy rice fields by applying machine learning algorithms to multi-temporal Sentinel-1A and Landsat data. International Journal of Remote Sensing 39(4), 1042–1067, https://doi.org/10.1080/01431161.2017.1395969.

Shen, N., Tan, J., Wang, W., Xue, W., Wang, Y., Huang, L., Gang, Y., Song, Y., Li, L. (2024): Long-term changes of methane emissions from rice cultivation during 2000–2060 in China: Trends, driving factors, predictions and policy implications. Environment International 191: 108958, https://doi.org/10.1016/j.envint.2024.108958.

Small, D. (2011): Flattening Gamma: Radiometric Terrain Correction for SAR Imagery. IEEE Transactions on

Geoscience and Remote Sensing 49(8), 3081–3093, https://doi.org/10.1109/TGRS.2011.2120616.

Surendran, U., Raja, P., Jayakumar, M., Subramoniam, S. R. (2021): Use of efficient water saving techniques for production of rice in India under climate change scenario: A critical review. Journal of Cleaner Production 309: 127272, https://doi.org/10.1016/j.jclepro.2021.127272.

Tucker, C. J. (1979): Red and photographic infrared linear combinations for monitoring vegetation. Remote Sensing of Environment 8(2), 127–150, https://doi.org/10.1016/0034-4257(79)90013-0.

Udimal, T. B., Jincai, Z., Ayamba, E. C., Owusu, S. M. (2017): China's water situation; the supply of water and the pattern of its usage. International Journal of Sustainable Built Environment 6(2), 491–500, https://doi.org/10.1016/j.ijsbe.2017.10.001.

Veloso, A., Mermoz, S., Bouvet, A., Le Toan, T., Planells, M., Dejoux, J. F., Ceschia, E. (2017): Understanding the temporal behavior of crops using Sentinel-1 and Sentinel-2-like data for agricultural applications. Remote Sensing of Environment 199, 415–426, https://doi.org/10.1016/j.rse.2017.07.015.

Wu, B., Zhang, M., Zeng, H., Tian, F., Potgieter, A. B., Qin, X., Yan, N., Chang, S., Zhao, Y., Dong, Q., Boken, V., Plotnikov, D., Guo, H., Wu, F., Zhao, H., Deronde, B., Tits, L., Loupian, E. (2023): Challenges and opportunities in remote sensing-based crop monitoring: a review. National Science Review 10(4): nwac290, https://doi.org/10.1093/nsr/nwac290.

Xiao, X., Boles, S., Frolking, S., Li, C., Babu, J. Y., Salas, W., Moore, B. (2006): Mapping paddy rice agriculture in South and Southeast Asia using multi-temporal MODIS images. Remote Sensing of Environment 100(1), 95–113, https://doi.org/10.1016/j.rse.2005.10.004.